Analysis of optical brain signals using connectivity graph networks

Marco A. Pinto-Orellana[1][0000−0001−6495−1305] and Hugo L. Hammer[2,3][0000−0001−9429−7148]

[1] Department of Mechanical, Electronics and Chemical Engineering, Faculty of Technology, Art and Design. Oslo Metropolitan University. marcop@oslomet.no
[2] Department of Information Technology, Faculty of Technology, Art and Design. Oslo Metropolitan University.
[3] Simula Metropolitan Center, Oslo Metropolitan University. hugoh@oslomet.no

Abstract. Graph network analysis (GNA) showed a remarkable role for understanding brain functions, but its application is mainly narrowed to fMRI research. Connectivity analysis (CA) is introduced as a signal-to-graph mapping in a time-causality framework. In this paper, we investigate the application of GNA/CA in fNIRS. To solve the inherent challenges of using CA, we also propose a novel metric: a maximum cross-lag magnitude (MCLM) that efficiently extracts major causality information. We tested MCLM in four types of cognitive activities (mental arithmetic, motor imagery, word generation, and brain workload) from 55 participants. CA/MCLM showed a compelling modeling capacity and revealed unexpected cross-subject network patterns. We found that motion imagery and mental arithmetic share a background network structure, and that the right prefrontal cortex, in AFp8, is an invariable destination for information flows in every stimuli and participant. Therefore, CA/MCLM-fNIRS showed potential for its use along with fNIRS in clinical studies.

Keywords: Brain signals, fNIRS, graph network analysis, connectivity analysis.

1 Introduction

Time-frequency analysis of biomedical signals is a traditional and fundamental mechanism in the evaluation and interpretation of brain activity [20]. In the past decade, the advances in computing processing increased the interest of further types of analysis, in particular those that offered models of the connections between brain regions. Thus, outcomes from classical graph theory could be used in biomedical research. Graph, a.k.a network, analysis (GNA) represents the relationships between node entities (electrode channels, or brain regions in biomedical signals). However, the method to convert multivariate time series into a single network graph is an open problem, because compared with other types of data, interpretability is highly relevant and essential. GNA in brain research,

mostly in functional magnetic resonance imaging (fMRI) studies, relies on connectivity analysis (CA) for this mapping. CA is a robust technique that can map any time series (under mild conditions) to a graph network through cross-time dependencies between a set of signals. In this mapping, a link (edge) between a node A and B describes an amount of signal causal information that circulates from A to B [23]. This relationship with causality in the time series domain is based on the Granger's definition of causality: a measure of the influence of a time series on the future values of another signal that cannot be explained the latter itself [9]. This joint use of GNA/CA has shown an impressive role in understanding and describing brain functions and dynamics [1].

We can distinguish three levels of connectivity: a) structural connectivity (SC) that is associated to the anatomical or physical linkages among brain regions; b) functional connectivity (FC) as the undirected, or symmetric, interaction map generated by the linear correlations between unexplained stochastic oscillations in the observed time series; and c) effective connectivity (EC) as the directed graph network constructed by measures of the time-causality (Granger-causality) that each signal has over the other observed channels [23,1]. These three degrees of connectivity yield practical knowledge about the underlying brain interactions from different viewpoints. EC and FC show the information-level dynamics inside the brain (FC highlights the correlation between channels, while EC focuses on their non-symmetric time-causality). Both are highly time-varying because of their dependency on external (stimuli) and internal factors. However, SC is the sole type of connectome that is almost constant over time, and it can only be reliably estimated through structural magnetic resonance imaging (sMRI) [8]. Nevertheless, we can infer EC and FC through (mid- or high-frequency sampled) electrical, magnetic, or optical signals [1].

Functional near-infrared spectroscopy (fNIRS) is a noninvasive method to quantify the hemodynamic changes in the brain using the absorption properties of the near-infrared (NIR) light waves (the spectral region in the range of 700nm and 900nm) [14]. Even though that fNIRS and fMRI shared the same goal of estimating hemodynamic changes, connectivity analysis has been widely used in fMRI, but only in a few studies with fNIRS signals: Liu et al. compared the statistical difference between the functional connectivity maps in a driving context against a resting state [13]; Behboodi et al. analyzed functional connectivity over fNIRS filtered through neural networks [3]. However, some recognized software packages, as the NIRS AnalyzIR toolbox, have also integrated some functions for inferring FC [18].

In this paper, we explore the use of connectivity analysis and GNA in fNIRS in order to reveal underlying brain dynamics. This application is not straightforward because of the processing challenges that are inherent to fNIRS with respect to fMRI: ten times higher sampling rate and high dimensionality. Even though that fMRI data is highly dimensional, the extracted time courses are restricted and summarized using specific regions of interest, typically defined through parcellation maps [6]. This anatomical clustering reduces the signal dimensionality substantially. However, in fNIRS, there is no standard anatomical

map that can be used for the same dimension-reduction purpose. Therefore, CA models incorporate a larger set of parameters when applied in fNIRS, and consequently, introduce interpretability issues. To solve this issue, we also propose a novel metric denoted as maximum cross-lag magnitude (MCLM) that summarizes CA parameters extracting the most significant causality information.

The rest of this paper is organized as follows: in section 2, we describe the formulation of CA and MCLM in a graph network framework. Later, in section 3, we describe the fNIRS data (4 cognitive activities, 9 events in 55 participants) where we tested our connectivity analysis proposal. In section 4, we describe the outcomes of our model and its implications. Finally, in section 5, we summarized the conclusions of our study.

2 Method

2.1 Model

Compared with machine learning methods, traditional time series models offer a slightly lower performance in prediction [10], but the latter keeps a robust and understandable model of the signals. This robustness property is advantageous in the analysis of biomedical signals because of the presence of several sources of artifacts, i.e., biological interference, device's mechanical noise, or other types of external noise [1]. In CA, the kernel technique is the vector (or multivariate) autoregressive model (VAR) [9] that models a set of M channels $\{X_1(t), X_2(t), \ldots, X_M(t)\}$ sampled every T_S seconds. Under this method, the observed value for a channel i at a time t is considered to be generated as a linear combination of the previous p points, of all M channels, and a stochastic increment $\varepsilon_i(t)$:

$$X_i(t) = \sum_{\ell=1}^{p} \sum_{j=1}^{M} \phi_{j\to i}^{(\ell)} X_j(t - \ell T_s) + \varepsilon_i(t) \quad i = 1, \ldots, M \tag{1}$$

In this notation, $\phi_{j\to i}^{(\ell)}$ measures the effect of the channel j at the time ℓT_s on channel i. The stochastic component $\varepsilon(t) = (\varepsilon_1(t), \varepsilon_2(t), \ldots, \varepsilon_M(t))^T$ is a multivariate white noise $\varepsilon(t) \sim \mathcal{N}(0, \Sigma_\varepsilon)$ with Σ_ε as the variance-covariance noise matrix, and $X\varepsilon(t)$ is uncorrelated with any previous point, $\mathbb{E}\left[\varepsilon(t)\,\varepsilon^T(t - \ell T_s)\right] = 0\,\forall \ell > 0$.

For a vectorial notation, let us define the multivariate recording at t as $X(t) = (X_1(t), X_2(t), \ldots, X_M(t))^T$, and the dependency matrix at lag ℓ:

$$\boldsymbol{\Phi}_\ell = \begin{pmatrix} \phi_{1\to1}^{(\ell)} & \phi_{1\to2}^{(\ell)} & \cdots & \phi_{1\to M}^{(\ell)} \\ \phi_{2\to1}^{(\ell)} & \phi_{2\to2}^{(\ell)} & \cdots & \phi_{2\to M}^{(\ell)} \\ \vdots & \vdots & \ddots & \vdots \\ \phi_{M\to1}^{(\ell)} & \phi_{M\to2}^{(\ell)} & \cdots & \phi_{M\to M}^{(\ell)} \end{pmatrix} = \left(\phi_{2\to1}^{(\ell)}\right)_{i,j=1\ldots M} \tag{2}$$

Then, the VAR model of Equation 1 can be expressed as a linear matrix combination,

$$X(t) = \sum_{\ell=1}^{p} \Phi_\ell X(t - \ell T_s) + \varepsilon(t) \quad i = 1, \ldots, M \tag{3}$$

We should remark that Σ_ε measures the linear covariance between the stochastic variations in the channels that are not explained by this model, i.e., it serves as a quantification of the functional connectivity among the measured channels [1].

The set of matrices $\Phi = \{\Phi_1, \Phi_2, \ldots, \Phi_M\}$ describes the magnitude of non-symmetrical temporal dependencies among the channels in the dataset. Therefore, these pieces of information can be employed to quantify the effective connectivity in the set of signals: a) in the time domain, these coefficients can estimate the time information flow between channels; b) in the frequency domain, these matrix set can estimate the cross-spectrum and determine the magnitude of information that circulates through frequency bands [1,23]. These possibilities allow us to use different metrics: partial directed coherence [2], directed transfer function [12], as well, other improved formulations [17].

Due to our current interest in time-domain characteristics, we introduce a simple metric derived from the VAR model: the maximum cross-lag magnitude (MCLM). MCLM is an operator $\mathbb{R}^{p \times p \times M} \to \mathbb{N}^{p \times p} \times \mathbb{R}^{p \times p}$ that maps the set Φ into a tuple (L, Θ) where L is the max-lag matrix, and Θ is the max-dependency matrix. L is defined as a $p \times p$ matrix where each item $l_{i,j}$ is the time lag with the strongest absolute coefficient ϕ:

$$l_{i,j} = \arg \max_{\ell=1,\ldots,p} \left| \phi_{i \to j}^{(\ell)} \right| \tag{4}$$

Θ is defined as a $p \times p$ matrix where each item is the cross-lag maximum coefficient between channel i and j:

$$\theta_{i,j} = \phi_{i \to j}^{(l_{i,j})} \tag{5}$$

Sample estimators of both parameters, $\hat{l}_{i,j}$ and $\hat{\theta}_{i,j}$ can be estimated from the data and their confidence interval obtained through subsampling Monte Carlo simulations given that the distributions of $\hat{\phi}_{i \to j}^{(\ell)}$ are known [4,16,15].

The MCLM max-lag matrix, Θ, can be interpreted as an adjacency matrix of a weighted graph network. Therefore, a graph $G_\Theta = (V, E, \omega)$ can be constructed where $V = 1, \ldots, M$ is the set of channels in the observations as vertices; E is the ordered set of edges or links $E \in V \times V$, and the weight function $\omega : E \to \mathbb{R}$ that assigns the maximum dependency magnitude $\theta_{i,j}$ as weight for the link $i \to j$. Furthermore, Σ_ε can also be reinterpreted as an undirected graph $G_\Sigma = (V, E, \omega)$ under a similar formulation.

Considering that a specific event for each subject τ will be associated with a matrix $\Theta^{(\tau)}$, we introduce two terms for further cross-subject analysis: a representative max-dependency matrix $\Theta^{(*)}$ as the average of all $\Theta^{(\tau)}$; and a coverage

Experiment	Events	Dataset	Participants	fNIRS Channels
N-back (NB)	0-back 2-back 3-back	NBWG	26	*Pre-frontal* (16): AF1, AF2, AF5h, AF6h, AF7, AF8, AFF3h, AFF4h, AFF5, AFF6, AFFz, AFp3, AFp4, AFp7, AFp8, AFpz. *Central region* (8): C3h, C4h, C5h, C6h, FCC3, FCC4, CCP3, CCP4. *Centro-parietal* (6): , CPP3, CPP4, P3h, P4h, P5h, P6h. *Parieto-occipital* (6): PO1, PO2, POOz, PPO3, PPO4, PPOz.
Word Generation (WG)	WG WG baseline			
Motor Imagery (MI)	Right MI Left MI	MIMA	29	*Pre-frontal* (7): AF1, AF2, AFp5h, AFp6h, AFp7, AFp8, AFpz. *Central region* (26): C3h, C4h, C5h, C6h, CCP1, CCP2, CCP3, CCP4, CCP5, CCP6, CP3h, CP4h, CP5h, CP6h, FC3h, FC4h, FC5h, FC6h, FCC1, FCC2, FCC3, FCC4, FCC5, FCC6, Fp1h, Fp2h. *Occipital* (3): O1h, O2h, POOz.
Mental Arithmetic (MA)	MA MA baseline			

Table 1. Experiments and events recorded in the two datasets. The number of participants and channels employed in the dataset are also indicated. Each fNIRS channel corresponds to the midpoint between the optical source and detector with the equivalent label according to the extended 10-20 EEG standard layout.

metric of each magnitude $\theta_{i,j}^{(*)}$ defined as the proportion of connections that are non-null:

$$\text{coverage}\left\{\theta_{i,j}^{(*)}\right\} = \frac{\left|\left\{\theta_{i,j}^{(\tau)} \neq 0 | \forall\tau\right\}\right|}{\left|\left\{\theta_{i,j}^{(\tau)} | \forall\tau\right\}\right|} \tag{6}$$

2.2 Data description

In order to show the expressiveness and capabilities of the model in fNIRS signals, we used two recorded datasets by Shin et al. [19,11] . These sources of data are publicly available and contribute to the reproducibility of the results with the presented model. Even though that both datasets contain other non-optical biomedical signals, we restricted to the analysis of their fNIRS time series.

In the first dataset (NBWG), twenty-six participants were requested to perform three cognitive activities (n-back, word generation, and discrimination/selection response task) from which we selected two relevant activities for our goals [11]:

- *N-back tasks (NB).* In this exercise, every participant performed a 0-, 2-, or 3-back task during 60 seconds (40 seconds for the activity, and 20 seconds for the resting period). The experiment is organized in three sessions, wherein each session, nine n-back tasks were performed (3 times per n-back type) in a counter-balanced order per session.
- *Word generation activity (WG).* In three sessions, consisting of twenty trials each one, the subjects were presented a single letter for WG or a fixation-cross in a screen for baseline. The task included 10 seconds for the task and 13-15 seconds for a resting interval.

In the second data source (MIMA), twenty-nine subjects performed two types of activities that represent typical mental tasks commonly used in brain-computer studies [19]:

- *Motor imagery (MI).* MI is a classical test for brain-computer interfaces for different purposes: computer-assisted rehabilitation, games, and virtual reality systems. In MIMA, all participants performed a mental process consisting of imaging the scene of opening and closing their hands while grabbing a ball. They were also requested to imagine this movement with a speed of one cycle per second. The experiment was organized in three sessions, with ten trials for left hand MI, and ten trials for right hand MI.
- *Mental arithmetic (MA).* In this activity, the subjects were requested to subtract a one-digit number from a three-digit number in the lapse of twelve seconds (two seconds for displaying the instruction, and ten for solving it) with a resting time of 15-17 seconds. This session was repeated 20 times per subject.

Further details about the datasets, and experimental designs, we refer to [11] and [19].

2.3 Data analysis

The biomedical signals from MIMA and NBWG datasets were processed according to the steps as follows:

1. Signals are subsampled in MIMA from 12.5Hz to 10Hz in order to ensure the same sampling frequency across datasets.
2. Time series are frequency filtered in the range 0.01-0.1Hz using a finite impulse filter of 100th order. The extracted spectral range is typically associated with cerebral autoregulation, cognition, and neural activity [14].
3. Signals are partitioned into sections according to their recorded time events.
4. A VAR(20) model is fit for each segment allowing to model dependencies up to 2 seconds in the past, removing the estimated parameters with p-values greater than 0.0001. The remaining estimated components have strong evidence to be non-null, and therefore, are appropriate for our analysis.

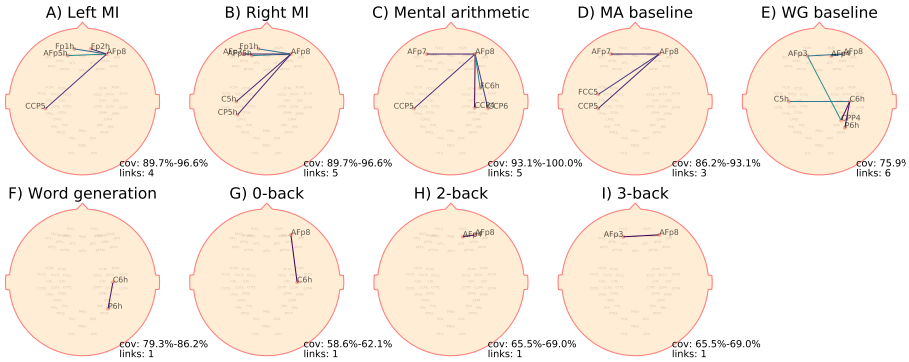

Fig. 1. General connections in the functional connectivity.

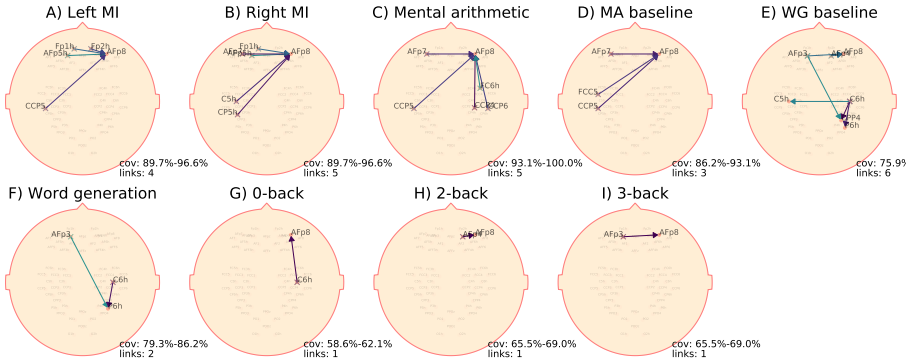

Fig. 2. General connections in the effective connectivity using MCML. Note that MCLM as a connectivity metric is able to capture the same links than raw effective connectivity, as it is shown in Figure 1.

5. Matrix Θ and L, and the link coverages are calculated according to Equations 4, 5 and 6.
6. The approximate distribution for each coefficient θ_{ij} was estimated using a Monte Carlo simulation and a subsampling as described in [15] and [16].
7. The mean magnitude for each link is estimated across all subjects as well as their approximated distribution.
8. For our exploratory analysis, we calculate two primary metrics: centrality and information flow. We refer to [8] for a more comprehensive review of alternative network graph metrics.

3 Results and discussion

Based on the described procedure, a network map was estimated for each event and person (246 networks in total). This large amount of data motivated us

to reduce the parameters to analyze and describe in a concise but informative manner.

3.1 Cross-subject general connections

A link was considered general if their coverage is above the 95% percentile in the network graph related to a specific stimulus/event. No general coverage threshold was used because the maximum coverage in the data can be lower than 100% (as a direct consequence of the p-value filtering of step 5 in section 2.3). Although the uncertainty-based filtering increased the confidence of the link magnitudes estimated, it also removed relevant connections that present high levels of uncertainty.

The most significant directed and undirected connections (effective and functional connectivity) are displayed in Figure 2 and Figure 1, respectively. Most connections in both types of connectivity metrics were similar. Moreover, this analysis allowed us to interpret the effect of the information flow between brain regions using the directed links:

- In MI activites, it is observed that data flows were originated in the opposite hemisphere of the imagined motion hand, i.e., the left MI had a dependency link from the right to left hemisphere, and vice-versa.
- MA tasks always exhibit a link in the right hemisphere between the central-parietal region towards the prefrontal cortex. In comparison, its baseline MA denoted a similar link but starting from the left hemisphere.
- WG experiment shows relevant flows in the right central, parietal, and left prefrontal cortex, but with an additional link from the left prefrontal cortex. We should emphasize that the activity on the central-parietal region was confirmed as activated areas in WG tasks through an fMRI study by Brannet el al. [5],
- Attention tasks (0-back) appeared to have similar information flows compared with MA, while mental workload (2-back and 3-back) data flows were strongly evident only in the prefrontal cortex.
- It is worth mentioning that, in all cases, numerous data flows seemed to be oriented towards the right hemisphere. This phenomenon can be associated with the fact that the participants were mostly right-handed. However, further research is needed to ratify this hypothesis.

3.2 Cross-subject common connections

We define a link as common if their coverage in the dataset is above the median of the signal amplitude on the event's coverage. The common links in effective connectivity are shown in Figure 3. Compared with the network maps in Figure 2, these maps can be slightly different, because of the presence of frequent, but not general, links.

Maps of common links allowed us to observe more details about the reconfiguration of the connectivity in the brain under different experimental tasks.

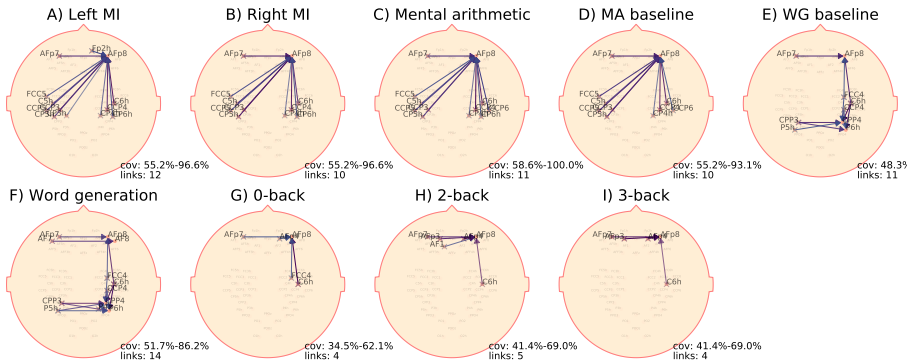

Fig. 3. Common connections in the effective connectivity

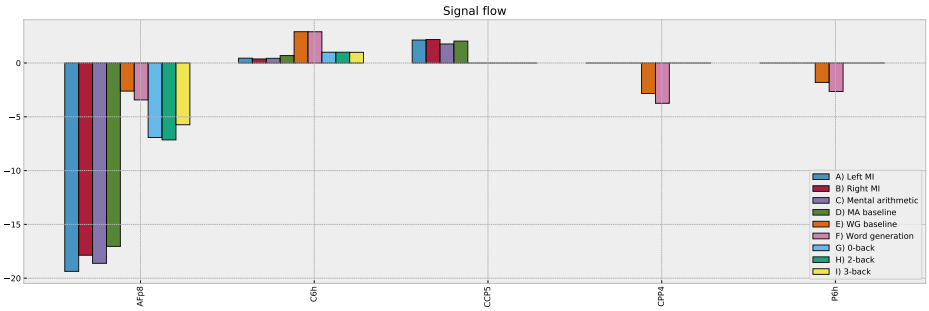

Fig. 4. Net information flow. The most significant NIF values (NIF > 2) are displayed (channel AFp8, C6h, CCP5, CPP4, P6h) and classified according to the datasets' events: A) Left MI, B) Right MI, C) Mental arithmetic, D) MA baseline, E) WG baseline, F) Word generation, G) 0-back, H) 2-back, and I) 3-back.

Connectivity maps showed a natural organization intro three large groups, or clusters, of tasks: mental activity (mental imagery and arithmetic), verbal fluency (word generation and its baseline), and mental workload (0-, 2-, and 3-tasks).

All connectivity maps showed a "gravity effect" of the electrode AFp8 (right prefrontal cortex): it is the preferred destination point for all the data flows in every event of each subject in the datasets. The influence of the right prefrontal cortex was denoted in MA tasks by Tanida et al. [21], in MA in a study by Ehrlichman et al. [7], and in n-back tasks according to Vermeij et al. [22].

3.3 Net information flow

For a node (channel) i, net information flow (NIF) is defined as the total flow that enters into the node (out-flow) subtracted from the total flow originated in

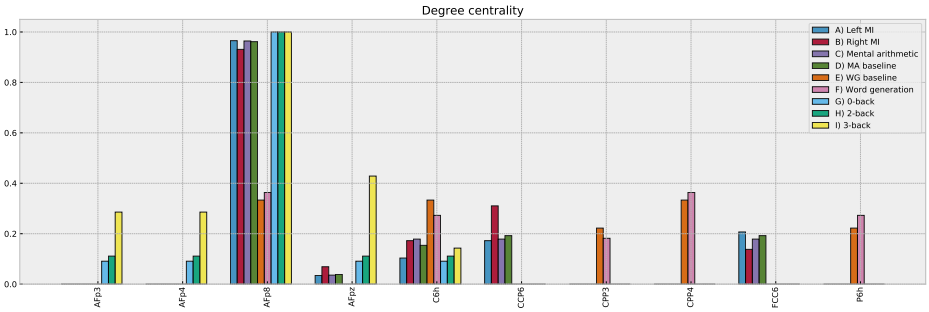

Fig. 5. Network degree centrality. The most significant NDC values (NDC > 0.2) are shown (channels AFp3, AFp4, AFp8, AFpz, C6h, CCP6, CPP3, CPP4, FCC6, and P6h). Each bar corresponds to the NDC of datasets' event: A) Left MI, B) Right MI, C) Mental arithmetic, D) MA baseline, E) WG baseline, F) Word generation, G) 0-back, H) 2-back, and I) 3-back.

the node (in-flow):

$$\mathrm{NIF}_i = \sum_{v \in V} \theta_{i \to v} - \sum_{v \in V} \theta_{v \to i} \tag{7}$$

This property estimates the final impact that the electrode had in the connectivity network. The electrode channel shows a higher dependency on the other channels when the net flow is negative; otherwise, it exhibits a particular impact on the network. The most relevant channels' NIF is shown in Figure 4. As it was discussed before, AFp8 was the electrode that is more influential on the network. However, its dependency magnitude varies according to the type of activity, demanding mental tasks, and effortless lexical tasks. It is also remarkable that the net information flow can provide insights to identify the type of task: lexical activities have a notable dependent effect in the right hemisphere (channel CPP4 and P6h), while mental tasks have a more role as sources' flow in the left hemisphere (channel CCP5).

3.4 Network degree centrality

For each node i, degree centrality (NDC) is defined as the proportion of information flows that have i as a source or destination with respect to the total links in the network:

$$\mathrm{NDC}_i = \frac{\sum_{v \in V} \mathbb{I}\left[\theta_{i \to v} \neq 0\right] - \sum_{v \in V} \mathbb{I}\left[\theta_{v \to i} \neq 0\right]}{\sum_{i \in V} \sum_{j \in V} \mathbb{I}\left[\theta_{i \to j} \neq 0\right]} \tag{8}$$

where $\mathbb{I}\left[\cdot\right]$ is the indicator function: $\mathbb{I}\left[x\right] = \begin{cases} 1 & x \text{ is true} \\ 0 & \text{otherwise} \end{cases}$.

The results are shown in Figure 5. In concordance with the previous assessments, the centrality role of the channel AFp8 is general across all experimental

tasks. However, a partial relevance is displayed for channel AFpz, CPP4, and CCP6, in mental workload, lexical, and MI/MA tasks, respectively.

4 Conclusions

Biomedical time series are often analyzed through their time changes or their spectral responses. Other types of analysis, such as network analysis, are usually only performed in fMRI data, where cross-dependency patterns are used to create and study brain graph networks. This signal-to-graph transformation is based on connectivity analysis (CA) and allows us to create complex network structures that associate sets of time series in a time-causality framework. Despite its proven effectiveness in fMRI, this methodology was not completely explored in optical biomedical signals.

In this paper, we investigated the possibilities of using CA with a new connectivity metric based on the classical, but robust, multivariate autoregressive model. This metric, a maximum cross-lag magnitude, relates each pair of signal channels with a quantified inter-channel time-dependency measure. We applied this formulation into fNIRS signals (from two different datasets) that contained four types of cognitive activities (mental arithmetic, motor imagery, word generation, and brain workload) organized into nine different categories of events. Each event was repeated at least four times in 55 participants (distributed in 26 participants in the first dataset and 29 in the second one).

Combining CA with our connectivity metric showed a compelling modeling potential and allowed us to reveal unexpected cross-subject dynamic causality patterns. Our results showed that motion imagery shares a similar background structure with mental arithmetic tasks; while channel AFp8 is always a destination for information flows regardless of the stimuli or participant. Simultaneously, the method provided event-related individual patterns that let to identify each event individually using some simple network properties. These results offer exciting possibilities for further extensions as complementary input in machine learning algorithms as well as possible clinical applications due to the availability of uncertainty measures of each dependency magnitude and the selection of potential regions of interest for more comprehensive MRI analysis.

5 Acknowledgments

This work is financially supported by the Research Council of Norway to the Project No. 273599, "Patient-Centric Engineering in Rehabilitation (PACER)".

References

1. A. R. Anwar, M. Muthalib, S. Perrey, A. Galka, O. Granert, S. Wolff, U. Heute, G. Deuschl, J. Raethjen, and Muthuraman Muthuraman. Effective connectivity of cortical sensorimotor networks during finger movement tasks: A simultaneous fNIRS, fMRI, EEG study. *Brain Topography*, 29(5):645–660, jul 2016.

2. Luiz A. Baccalá and Koichi Sameshima. Partial directed coherence: a new concept in neural structure determination. *Biological Cybernetics*, 84(6):463–474, may 2001.
3. Bahareh Behboodi, Choim Ji-Woong, and Jeon Hyeon-Ae. *Deep Neural Networks for Assessing Functional Connectivity: an fNIRS Study*. PhD thesis, Daegu Gyeongbuk Institute of Science and Technology, 2018.
4. Zdravko Botev and Pierre L'Ecuyer. Simulation from the tail of the univariate and multivariate normal distribution. In *Systems Modeling: Methodologies and Tools*, pages 115–132. Springer International Publishing, oct 2018.
5. John H Brannen, Behnam Badie, Chad H Moritz, Michelle Quigley, M Elizabeth Meyerand, and Victor M Haughton. Reliability of functional mr imaging with word-generation tasks for mapping broca's area. *American Journal of Neuroradiology*, 22(9):1711–1718, 2001.
6. Jingyuan E. Chen and Gary H. Glover. Functional magnetic resonance imaging methods. *Neuropsychology Review*, 25(3):289–313, aug 2015.
7. Howard Ehrlichman and John Barrett. Right hemispheric specialization for mental imagery: A review of the evidence. *Brain and Cognition*, 2(1):55–76, January 1983.
8. Farzad V. Farahani, Waldemar Karwowski, and Nichole R. Lighthall. Application of graph theory for identifying connectivity patterns in human brain networks: A systematic review. *Frontiers in Neuroscience*, 13, jun 2019.
9. Rainer Goebel, Alard Roebroeck, Dae-Shik Kim, and Elia Formisano. Investigating directed cortical interactions in time-resolved fMRI data using vector autoregressive modeling and granger causality mapping. *Magnetic Resonance Imaging*, 21(10):1251–1261, dec 2003.
10. Junhui Guo. Oil price forecast using deep learning and ARIMA. In *2019 International Conference on Machine Learning, Big Data and Business Intelligence (MLBDBI)*. IEEE, nov 2019.
11. Jaeyoung Shin and Alexander von Luhmann and Do-Won Kim and Jan Mehnert and Han-Jeong Hwang and Klaus-Robert MÃŒller. Simultaneous acquisition of EEG and NIRS during cognitive tasks for an open access dataset. *Scientific Data*, 5(1), feb 2018.
12. M. J. Kaminski and K. J. Blinowska. A new method of the description of the information flow in the brain structures. *Biological Cybernetics*, 65(3):203–210, jul 1991.
13. Zhian Liu, Ming Zhang, Gongcheng Xu, Congcong Huo, Qitao Tan, Zengyong Li, and Quan Yuan. Effective connectivity analysis of the brain network in drivers during actual driving using near-infrared spectroscopy. *Frontiers in Behavioral Neuroscience*, 11, oct 2017.
14. Paola Pinti, Felix Scholkmann, Antonia Hamilton, Paul Burgess, and Ilias Tachtsidis. Current status and issues regarding pre-processing of fNIRS neuroimaging data: An investigation of diverse signal filtering methods within a general linear model framework. *Frontiers in Human Neuroscience*, 12, jan 2019.
15. Dimitris N Politis, Joseph P Romano, and Michael Wolf. *Subsampling*. Springer Science & Business Media, 1999.
16. Joseph P. Romano and Michael Wolf. Subsampling inference for the mean in the heavy-tailed case. *Metrika*, 50(1):55–69, nov 1999.
17. C. Sandhya, G. Srinidhi, R. Vaishali, M. Visali, and A. Kavitha. Analysis of speech imagery using brain connectivity estimators. In *2015 IEEE 14th International Conference on Cognitive Informatics & Cognitive Computing*. IEEE, jul 2015.
18. Hendrik Santosa, Xuetong Zhai, Frank Fishburn, and Theodore Huppert. The NIRS brain AnalyzIR toolbox. *Algorithms*, 11(5):73, may 2018.

19. Jaeyoung Shin, Alexander von Luhmann, Benjamin Blankertz, Do-Won Kim, Jichai Jeong, Han-Jeong Hwang, and Klaus-Robert Muller. Open Access Dataset for EEG+NIRS Single-Trial Classification. *IEEE Transactions on Neural Systems and Rehabilitation Engineering*, 25(10):1735–1745, oct 2017.
20. Abdulhamit Subasi. Biomedical signal analysis and its usage in healthcare. In *Biomedical Engineering and its Applications in Healthcare*, pages 423–452. Springer Singapore, 2019.
21. Masahiro Tanida, Kaoru Sakatani, Ruriko Takano, and Keiko Tagai. Relation between asymmetry of prefrontal cortex activities and the autonomic nervous system during a mental arithmetic task: near infrared spectroscopy study. *Neuroscience Letters*, 369(1):69–74, October 2004.
22. Anouk Vermeij, Roy P. C. Kessels, Linda Heskamp, Esther M. F. Simons, Paul L. J. Dautzenberg, and Jurgen A. H. R. Claassen. Prefrontal activation may predict working-memory training gain in normal aging and mild cognitive impairment. *Brain Imaging and Behavior*, 11(1):141–154, February 2016.
23. Peter Zeidman, Amirhossein Jafarian, Nadège Corbin, Mohamed L. Seghier, Adeel Razi, Cathy J. Price, and Karl J. Friston. A guide to group effective connectivity analysis, part 1: First level analysis with DCM for fMRI. *NeuroImage*, 200:174–190, oct 2019.